Chapter IV

Design and Development of Lactoferrin Conjugated Lipid-polymer Nano-bio-hybrid for Cancer Theranostics

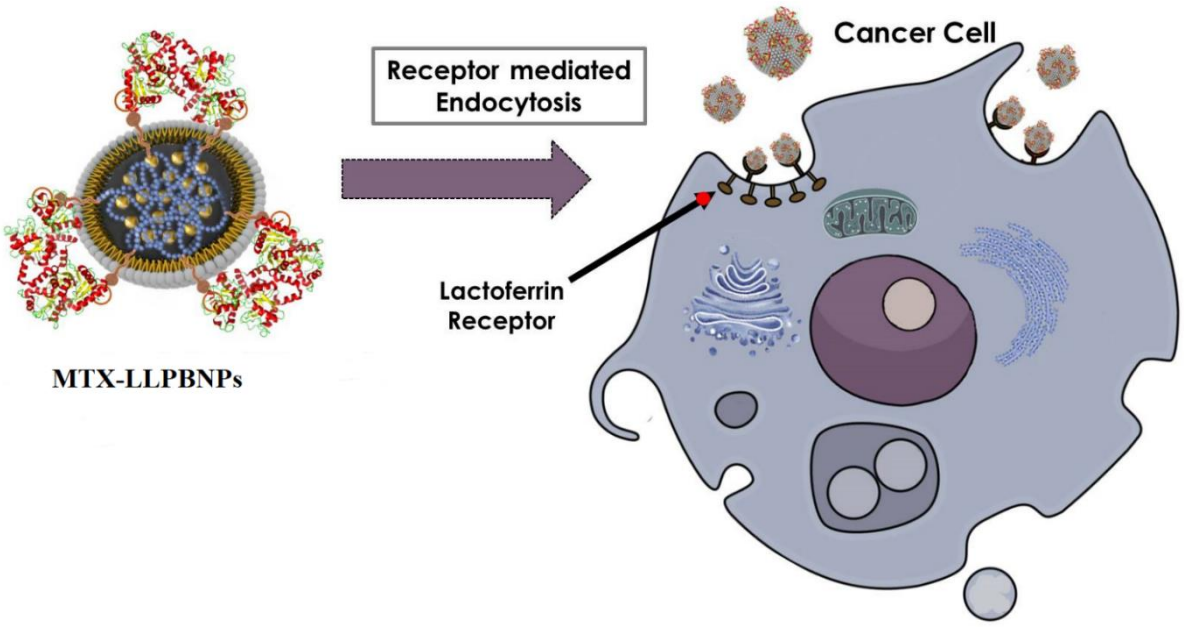

Rahul Kumar et al., ***Materials Today Communications.****31(2022) 103548:*
doi.org/10.1016/j.mtcomm.2022.103548

Candidate CRediT and collaborators contribution statement

Rahul Kumar: Data curation, formal analysis, investigation, methodology, writing – thesis, review & editing, and Conceptualization.

Collaborators: Review & editing, resource, validation, and software.

1. Introduction

One of the major applications of nanobiotechnology enables the controlled delivery of therapeutic drugs to the targeted site. In recent times, such controlled drug delivery carriers have improved drugs therapeutic index and pharmacokinetic properties for wider applications **[1]**. Over the decades, a large number of nanomedicines have been accepted commercially for various disease treatments. To date, approximately sixteen hundred liposomal drugs have been recruited for various clinical phase trials **[2]**. Nano-carriers have numerous advantages over free drugs as a delivery system. It facilitates sustained drug release due to polymer degradation over time, improved solubility of poorly water-soluble therapeutics, better drug accumulation inside the cells, reduced drug clearance, and co-delivery of more than one type of drug **[3]**. Due to their possible cytotoxicity in the human body and other biological systems, nano-carriers may cause systemic side effects. Nano-carriers, in particular, have the potential to damage cells by adhering to the surfaces of cellular membranes via electrostatic interactions or adsorption **[4,5]**. On the other hand, nano-fabrication of various nanoparticles (NPs) facilitates the protection of the drugs from the cellular environment, enhances cell specificity, and reduces cell cytotoxicity **[6,7]**.

In general, the nano-carriers under examination can be split into two categories: polymer and lipid-based NPs. Depending on the types of phospholipids used during synthesis of lipid-based NPs, the monomers of lipid may arrange in various structural forms, for instance, liposomes, solid lipid nanoparticles, nanostructured lipid particles, etc. used. Due to their great biocompatibility, attractive pharmacokinetic profile, high transport efficiency, and ease of surface application, they have been widely employed in cancer theranostics in recent years **[8]**. In addition to these advantages of lipids, certain limitations are also associated with them, e.g., they facilitate the fast drug release, their instability in long storage conditions, and low percent of drugs encapsulation **[9]**. However, polymer-based NPs have presented a promising

platform for drug delivery. They offer acceptable size, improved encapsulation efficiency, high cellular uptake, uniform drug release, enhanced physicochemical and pharmaceutical behavior, and reduced storage instability **[10]**. Hence, in the present study, it has been thought of developing a unique system comprising two different NPs. This dihybrid system comprising two NPs may be more promising than achieved due to their synchronous effects. Such a dihybrid system is synthesized using a strategic-based assembly process in which lipid monomer forms the shell surrounding the polymeric NPs in the system's core. This type of drug delivery system is a so-called lipid polymer-based NPs(LPBNPs). The above formulations overcome the negative attributes of lipid and polymer, as discussed earlier. It has also been reported that such a hybrid polymeric system may enhance the stability with increased circulation time of the drugs **[11,6]**. Two techniques can be employed to perceive the lipid-polymer hybrid construct viz., (i) the two-step nanoprecipitation method and (ii) the one-step nanoprecipitation method. The one-step precipitation method controls the pharmaceutical and physiochemical attributes, and the scale-up process is easier and more cost-effective **[11,12,13]**. Site-specific targeting and reducing cytotoxicity of the free drugs can be achieved using molecular probes and specific ligands by coupling them with the surface of the hybrid system. Such a conjugating hybrid system provides a promising strategy as a theranostic module that can easily detect and accumulate the drug to surface-expressed cancer cells. In this direction, various probes or ligands have been used for detecting malignant cells. Among the ligands, lactoferrin is one of the promising conjugating molecules because it has a high affinity for lactoferrin receptors and specifically binds to these molecules **[14]**. Numerous human malignancies, including breast cancer, ovarian cancer, and oral epidermoid carcinoma, overexpress lactoferrin receptors on their cell surface **[15]**.

Here, in the present study, we attempted to construct the ligand conjugated hybrid NPs for site-specific drug delivery and improve their effectiveness. The biodegradable polymer

polycaprolactone (PCL) has been employed in the core with methotrexate (MTX) as a potential anti-cancerous drug in the formulation. Further, soya lecithin containing stearic acid form the shell and surrounds the PCL core in the system. Stearic acid is anchored on the surface of LPBNPs through charge interaction, and lactoferrin is coupled to stearic acid through classical bioconjugation chemistry-based cross-linking **[16]**. It is possible to hypothesize that the MTX-laden LPBNPs (MTX-LPBNPs) and MTX-laden lactoferrin conjugated LPBNPs (MTX-LLPBNPs) may integrate the key characteristics of lipids and PCL for the development of a potent theranostics module.

2. Materials and methods

2.1 Materials

Methotrexate hydrate was obtained from Santa Cruz Biotechnology. Soya lecithin, stearic acid, lactoferrin were obtained from Sigma-Aldrich (USA). Chemicals for cell culture, which includes (DMEM-AT219) Dulbecco's Modified Eagle Medium, antibiotic solution 100X liquid streptomycin (10.0 mg/mL of 0.90 % normal saline sterilized); penicillin (10,000 U) (A001), L-glutamine trypsin-EDTA solution TCL007 (1X), PBS (phosphate buffer saline TL1101-5X 100.0mL), MTT (500.0 mg , thiazolyl blue tetrazolium bromide, TC 191), FBS (fetal bovine serum, RM10685-500mL), 4.0 % of paraformaldehyde (TC 119), DAPI (4,6-diamidino-2-phenylindole, TC229), triton 100X (TC286-500 ML), dimethyl sulphoxide (DMSO, TC185-100.0ml), sodium pyruvate were procured from HiMedia. 12-well plate, centrifuge tube, (EDC.HCL)1-ethyl-3-(3-dimethyl aminopropyl) carbodiimide hydrochloride, and (NHS) N-hydroxy succinimide were obtained from Merck. Absolute alcohol (99.90 %), and distilled water were used in all the experiments.

2.2. Fabrication of LPBNPs

The LPBNPs fabrication was carried out using a facile one-step precipitation technique. The structural components in the LPBNPs fabrication were PCL, lecithin, stearic acid, and MTX. In brief, PCL (2.50 mg/mL) with MTX were dissolved in dimethylformamide to form a water-miscible organic phase. While preparing the aqueous phase, soya lecithin- stearic acid with the mass ratio of 85: 15 was taken in Milli-Q water and was sonicated under cold conditions. The sonicated suspension was melted above the phase conversion temperature of the lipids to make a jelly-like solution. The aqueous phase contains 30.0 % lipid by weight of total PCL. Further, the organic phase was added dropwise through a syringe (5.0 mL) in the aqueous phase under stirring conditions. A specific height of 20.0 cm was maintained while adding the oil phase to the aqueous phase. Further, the samples were centrifuged at 12,000.0 rpm for 12.0 minutes to separate the nano-formulations under cold conditions. Consequently, the samples were washed three times with double distilled water to remove the unbound chemicals. To protect the formulations from freezing, the washed sample was resuspended in the sucrose solution 2.0% (w/v). Finally, the samples were freeze-dried to form a powder and were kept in a desiccator at room temperature for further use.

2.3. Lactoferrin conjugation with MTX-LPBNPs

A typical bioconjugation procedure comprising EDC: NHS chemistry has been used in various studies to couple carboxyl and amino groups of the molecules **[16,17,18,19,20].** The stearic acid's amino group of lactoferrin and carboxyl groups were conjugated through a covalent bond. Briefly, MTX-LPBNPs (12.0 mg) were dissolved in 2.0 mL of PBS. After that, MTX-LPBNPs were treated with 10 mM of EDC: NHS to activate its carboxyl groups for further complexation. Subsequently, the sample was incubated under the stirring condition of 800.0

rpm for 3.0 h at 25°C. Further, 1.5 mg/mL of lactoferrin was mixed with MTX- LPBNPs suspension at physiological pH followed by stirring for 6.0 h to achieve the proper conjugation. The conjugated MTX-LPBNPs were separated using cold centrifugation at 12,000.0 rpm for 20.0 minutes. The purified nanoformulation was cleaned three times with double distilled water to remove unbound lactoferrin. Finally, washed nanoformulation was freeze-dried using a lyophilizer and kept in desiccator at room temperature. The detailed step-wise-step synthesis of lactoferrin conjugated MTX-LPBNCs and its cellular uptake through receptor mediated endocytosis has been illustrated in **Fig. 4.1**.

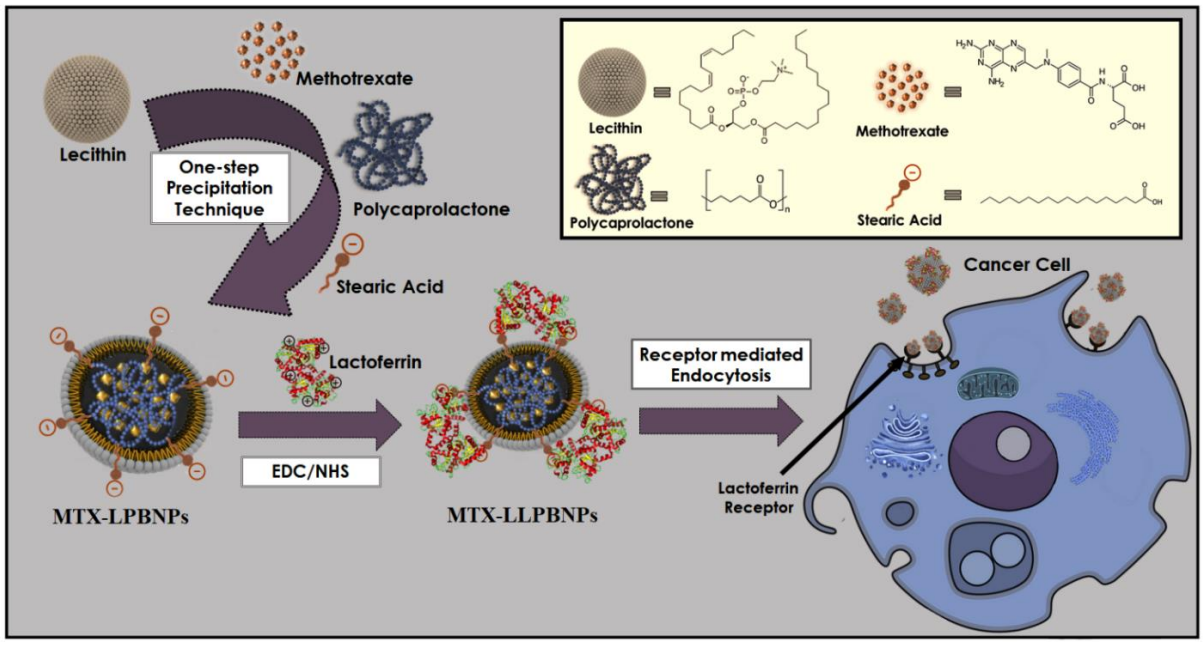

Figure 4.1. Schematic illustration of the synthesis of lactoferrin conjugated MTX-LPBNPs using one-step precipitation technique and its cellular internalization through receptor-mediated endocytosis.

2.4. Particle size analysis and assessment of surface charge using Zeta sizer

The particle size and charge distribution of the formulations were studied using a zeta sizer (Zetasizer Nano ZS90). Briefly, the solution of MTX-LPBNPs, and MTX-LLPBNPs was diluted ten times and sonicated for one minute individually since the size of the particle depends on its concentration. The samples were placed in the polystyrene cuvette, and it was scanned

using the laser beam to analyze the size and charge. The scanning of the sample was taken at an angle of 90° at room temperature.

2.5. Drug encapsulation efficiency (DEE)

The amount of MTX in MTX-LPBNPs and MTX-LLPBNPs was calculated with HPLC (High-performance liquid chromatography; HITACHI D-6500, Japan) furnished with a C18 column. In brief, 5.0 mg of MTX-LPBNPs and MTX-LLPBNPs were dissolved in phosphate buffer saline separately. After that, solutions were poured into a dialysis tube, a pore size distribution of 10 kDa. Dialysis was allowed under magnetic stir at 120.0 rpm against double distilled water. Dialysis was conducted for 1.0 h, and sink condition was maintained throughout the experiment to remove unentrapped MTX from the formulations. Further, 2.0 mL of recipient solution was taken periodically and restored with 2.0 mL of phosphate buffer to equilibrate the system. The resulting solution was poured into the HPLC vials and loaded into the HPLC system for further analytical investigation. The analytical validation of the HPLC method concerning selectivity, linearity, accuracy, repeatability, and intermediate precision was thoroughly conducted according to ICH guidelines.

2.6. Scanning electron microscopy (SEM)

The morphological characteristics, including the shape and size of the MTX-LPBNPs and MTX-LLPBNPs, were examined with SEM at the accelerated voltage of 26.0 kV. A small volume of formulations was taken individually and dried on a rectangular slide. The gold coating was applied to the sample to make it conductive. After that, the conductive sample was held on a copper stub, and images were taken.

2.7. Powder X-ray Diffractometry (XRD)

XRD was employed to investigate the crystal or polycrystalline nature of lyophilized powder of LPBNPs, and MTX-LLPBNs (Rigaku SmartLab 9Kw powder type, without an X cradle). A radiation source Cu Ka (λ=1.54Å) was used with a voltage of 30.0 kV to see the XRD pattern. X-ray scanning from initial angle 2θ = 10° to 2θ = 80° at a scanning speed of 0.03°/second yielded the diffractogram. All the experiments were performed at room temperature.

2.8. Fourier Transform Infrared Spectroscopy (FT-IR)

The FT-IR (Thermo Scientific™: Nicolet iS5) was used to study the chemical functionality through the spectrum analysis of MTX-LPBNPs and MTX-LLPBNPs. A hydraulic press (HP-15-TM; HP-mini) was used to make a 13.0 mm pellet with a force of 15.0 tones. The dried samples of the formulations were mixed with IR-grade potassium bromide to prepare pellets. The spectra of the formulations were recorded separately for all the formulations between wavenumber 4000 cm^{-1} and 800 cm^{-1}.

2.9. Methotrexate release profile

Zero and first-order kinetics models were applied to assess the drug's dissociation behavior from constructed MTX-LLPBNPs formulation. The drug dissociation from constructed NPs was examined for 200.0 h. In brief, 10.0 mg of MTX-LLPBNPs was taken in 3.0 mL of PBS containing 0.1% w/v Tween 80 (to maintain sink condition) at the neutral pH (7.4). After that, the solution was decanted inside the dialysis tube with a pore size distribution of 10 kDa. Since the experiment was performed in triplicates, the formulations were equally distributed in three dialysis tubes, each containing 3.0 mL of the sample. Dialysis was permitted against 100.0 mL of PBS at the physiological conditions. All three dialysis tubes were placed on a horizontal shaker for 200.0 h at 37°C at a rotating speed of 180.0 rpm. A portion of the sample was collected and replaced with the same amount of PBS at regular intervals. The obtained sample

was purified using centrifugation at 12,000.0 rpm for 15.0 min in cold conditions. The presence of the drug (MTX) was estimated by recording the absorbance at λ_{260} nm using a UV spectrophotometer, and the exact concentration was evaluated by comparing the absorbance with the standard calibration plot.

2.10. Storage stability

The final MTX-LLPBNPs were selected for storage stability performance following ICH guidelines. The sample was divided into two batches and kept in sealed vials at storage conditions of 4 °C and 25°C/60% RH (Relative Humidity) separately for 1 month and 3 months. Finally, storage performance was evaluated in percent encapsulation efficiency, particle size, PDI, and zeta potential.

2.11. Cell culture and assessment of *in vitro* cellular toxicity

A breast cancer cell line (MCF-7) was selected to investigate the cytotoxic effect of the developed hybrid-nano-bioconjugate. The cells were grown in DMEM supplemented with 1.0% streptomycin (10.0 mg/mL), 1.0% penicillin (10,000.0 U/mL), and 10.0% (FBS) fetal bovine serum. A CO_2 incubator (5.0% CO_2, 95.0% relative humidity, 37^0C) was used to incubate the cells. Subculturing was carried out until cell density reached 1×10^5 cells/mL in the culture flask. Further, cultured cells were taken in the 12.0 well plate containing nutrient medium and grown for 12.0 h. After that, the media was taken off, and a new medium comprising five treatment groups was taken in a culture plate (two sets). In the first, second, third, fourth, and fifth groups, the MTX at 2.0, 4.0, 6.0, 8.0, and 10.0 µg/mL were taken, respectively. A similar concentration of MTX was taken in each group in all the formulations. However, the LPBNPs were taken as a negative control in the group. Cells were incubated in the CO_2 incubator at 5.0% CO_2 and 37 °C for 24.0 h and 48.0 h of incubation, separately to validate the *in vitro* analysis. In the next step, the media was removed from each well after the

completion of incubation, and subsequently, cells were cleaned three times to eliminate the residual amount of any free MTX, LPBNPs, MTX-LPBNPs, and MTX-LLPBNPs formulation. Further, the cells were seeded (12 well plates) in the complete growth medium comprising 5.0 mg/mL MTT previously prepared in PBS. After that, the plates were incubated for 4.0 h in a CO_2 incubator. After incubation, formazan crystals were formed inside the well, which is further, solubilized using DMSO (dimethyl sulfoxide), and the absorbance was recorded at λ_{570} nm using an ELISA plate reader (Synergy H1 hybrid, Biotek, USA model).

2.12. Fluorescence microscopy

Fluorescence microscopy was used to see the morphological changes of the cancer cells. The MCF-7 cells were seeded (1×10^5 cells/well) in 12-well plates (two sets) with a complete nutritional medium and incubated for 12.0 h in a CO_2 incubator. After that, the medium was taken off, and cells were cultivated with the fresh complete medium containing LPBNPs, MTX-LPBNPs, and MTX-LLPBNPs at equivalent MTX of 10.0 µg/mL. The plate was kept separately in the incubator for 24.0 h and 48.0 h. Following that, the nutrient medium comprising inducers in the wells was removed, and then the cells were rinsed three times using PBS to remove any remaining inducers. Subsequently, cells were fixed with 4.0% paraformaldehyde for 15.0 min at 25°C. The surface was washed three times with PBS to remove the unbound paraformaldehyde. Cells were incubated for 5.0 min with 0.1% (v/v) Triton X-100 followed by PBS washing to create the pores. After that, a 1.0% BSA solution was added to prevent nonspecific stain binding. The cells were rinsed three times with PBS to remove the unbound BSA. Finally, the cells were stained with DAPI (nuclei stain) and rhodamine-conjugated phalloidin (F-actin stain) sequentially, where 30.0 min incubation was provided for each staining. Finally, a fluorescence microscope (Nikon Ti-U) was used to capture the fluorescence images of DAPI (excitation/emission at $\lambda_{340\text{-}380}/\lambda_{460\text{-}500}$ nm) and

rhodamine-conjugated phalloidin (excitation/emission at λ_{552}/ λ_{578} nm) stained cells in a controlled environment.

3. Results and discussion

3.1. Particle size, Size distribution, the Surface charge of hybrid-nano-bioconjugate

The particle size and size distribution of MTX-LPBNPs, MTX-LLPBNPs were measured using a zeta sizer. The value of the polydispersity index (PDI) was calculated using the equation 1:

$$PDI = \frac{M_w}{M_n} \qquad \ldots\ldots\ldots Eq.\ 1$$

where, M_w and M_n denote weight-average molar mass and number average molar mass, respectively.

The detail of particle size and size distribution of the formulations are illustrated in **Table 4.1**. The general sizes of the particles are obtained in the range of 520–650 nm (**Fig. 4.2**) with a polydispersity of 0.144–0.163, which is not a very broad size distribution, indicating the precision in the fabrication of hybrid nano bioconjugate. The sizes noticed for the formulations are higher than those observed in previous studies in different formulations **[21]**. The higher molar ratio of soya lecithin, stearic acid, and polymer in the system is consistent with the increment in the size of the hybrid system. The final viscosity of the dispersion is increased with incremental changes in the amount of lipid-polymer content, which subsequently affects the size of hybrid nano bioconjugate **[22]**. Moreover, lactoferrin molecules significantly affect the formulations' size and increase their diameter. The characterization mentioned above suggests that there may be effective conjugation between the amino group of the lactoferrin and the carboxylic group of the stearic acid. This was also chemically confirmed using FTIR analysis, discussed in Section 3.4. Further, the size obtained through the zeta sizer differs from the size when evaluated using SEM. The above outcome is demonstrated in the fact of SEM governs the morphological size in a solid-state while the zeta sizer exposes the hydrodynamic

diameter in the aqueous phase **[23]**. PDI is an important parameter that gives information about particle size distribution. PDI value less than 0.2, indicates homogenous particle size distribution. The value of PDI of the formulated system is less than 0.2, which is comparable to other reported studies **[24]**. In the next step, the surface charge was calculated for the final MTX-LLPBNPs in the system comprising only MTX-LPBNPs for comparative study. The Zeta potential of a hybrid-nano-bioconjugate system in the medium is a significant indicator of stability, cell membrane interactions, and biological activity. The overall high value of zeta potential, either positive or negative, facilitates the strong repulsive forces among the carriers, preventing the agglomeration of the particles **[25]**. The negative charges on the nano bioconjugate surface are indicated by the zeta-potential illustrated in **Table 4.1**. The absolute value of the negative charge due to a phosphorous group of the lipid is bigger than the positive charge from the lactoferrin molecule **[26]**. Due to the overall negative charges of the carriers in an aqueous environment, the stability of the hybrid-nano-bioconjugate is enhanced

Table 4.1. Particle size, size distribution, zeta-potential, and drug encapsulation efficiency of MTX-LPBNPs and MTX-LLPBNPs and data represent mean ± SD, *n=3*

Sample	Particle size (nm)	Polydispersity	Zeta potential (mV)	Encapsulated efficiency (%)
MTX-LPBNPs	520.50 ± 3.86	0.144 ± 0.034	-27.10 ± 1.17	78.0 ± 2.4%
MTX-LLPBNPs	650.70 ± 4.90	0.163 ± 0.036	-20.72 ± 1.23	84.0 ± 3.2%

The encapsulated drug content within the constructed hybrid-nano-bioconjugate is a critical parameter to explain their diverse biological applications. The drug encapsulation efficiency was calculated using **Equation 2**.

$$\mathrm{DEE}(\%) = \frac{\text{Quantity of total drug} - \text{Quantity of free drug}}{\text{Quantity of the total drug}} \times 100 \qquad \ldots\ldots\ldots \textit{Eq. 2}$$

Table 4.1 shows the amount of drug encapsulated in LPBNPs and LLPBNPs systems which were found to be 78.0±2.4% and 84.0±3.2%, respectively. The obtained encapsulation efficiency for LLPBNPs systems is relatively higher than other delivery systems reported previously **[27,6]**. It is attributed to results that the drug encapsulation efficiency increases with the increase in the diameter of the carrier. This is also supported by the fact that as the structure's diameter grows, the specific surface area of the structure decreases. The reduced specific surface area further restricts the faster diffusion of drugs from NPs to mediums **[28]**. Further, the above results also interpret that a certain amount of drugs may adsorb on the surface of LLPBNPs *via* weak bonds like H-bond, Vander-wall forces, electrostatic interactions, etc. It is also hypothesized that the PCL may restrict the faster diffusion of drugs from polymeric core to lipid layers resulting in high encapsulation efficiency **[29]**.

Nevertheless, the tolerable DEE values demonstrate the efficacy of the hybrid-nano-bioconjugate in the loading of anticancer drugs. Such a hybrid-nano-bioconjugate system shows the possibility of a useful drug delivery carrier with appropriate size, charge, and drug loading efficiency. Further validation parameters such as selectivity, linearity, accuracy, repeatability, and intermediate precision for the HPLC method were thoroughly analyzed. The retention time of the MTX in formulated hybrid-nano-bioconjugates and various concentrations of free MTX were detected as 3.2 min proving selectivity of the method. The value of R^2 was found to be 0.98 indicating excellent linearity of the method, however, accuracy in terms of recovery of the MTX was estimated to be 99.8%. Further relative standard deviation values for repeatability (precision intra-assay) and intermediate precision (precision inter-assay) were found to be less than 5% confirming the method was more precise.

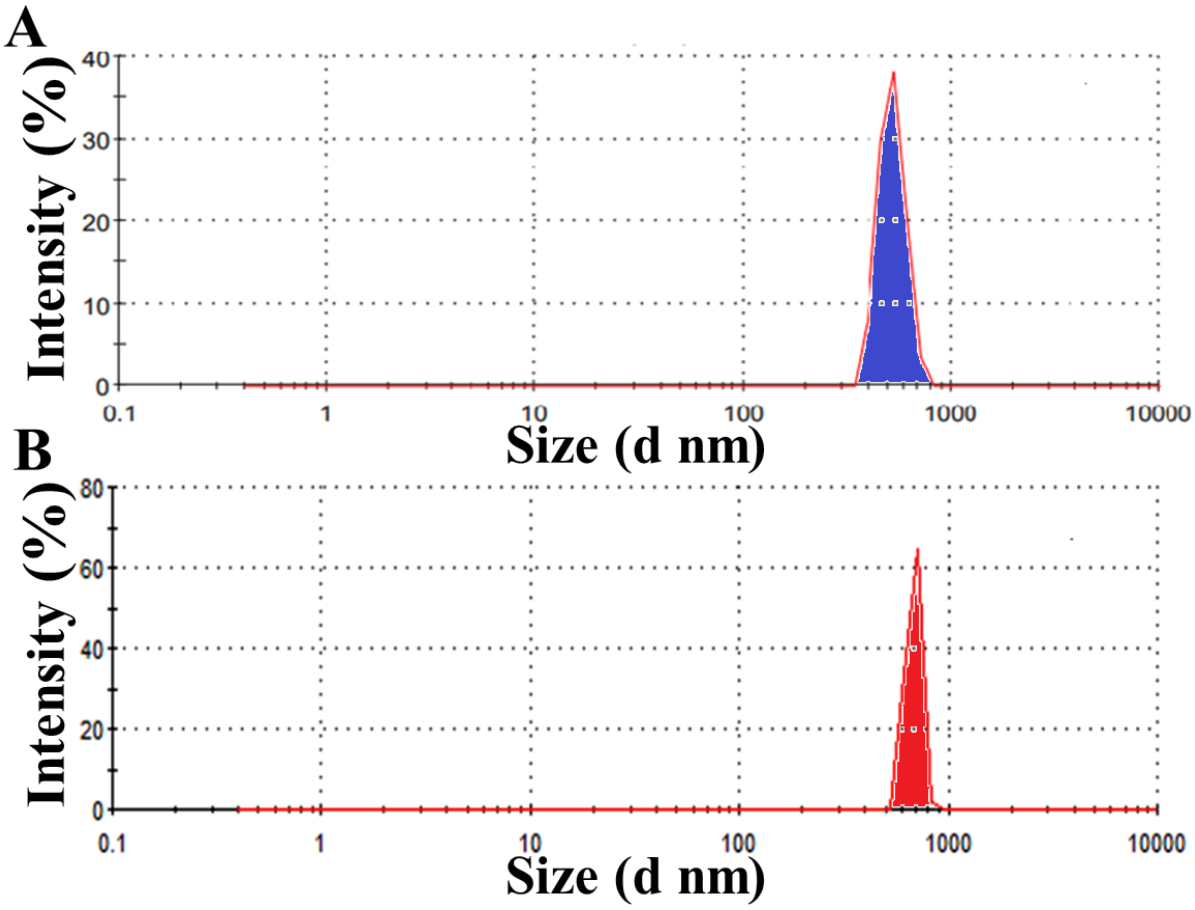

Figure 4.2. Distribution of hydrodynamic diameter in (nm) (A) MTX-LPBNPs and (B) MTX-LLPBNPs.

3.2. Analysis of morphological surface

The morphological surface of MTX-LPBNPs and MTX-LLPBNPs was studied using SEM characterization, as shown in **Fig. 4.3.** In both cases, overall spherical structures were observed, indicating the successful hybrid nano-bio carrier formulation through a nanoprecipitation technique. In the case of MTX-LPBNPs, the spherical structures were smooth and possessed a diameter in the range of 1.0 µm **(Fig. 4.3A).** Upon addition of lactoferrin onto MTX-LPBNPs, the size became relatively larger **(Fig. 4.3B).** The aforementioned results can be interpreted that the long chain of the polymer may arrange in the compact form of the polymer **[30]**. Consequently, the lipid monomer surrounding the polymer is aligned uniformly with the proper shape. The SEM image of the formulated NPs agrees with previously reported studies for

different hybrid NPs **[31]**. Further, the elemental analysis of MTX-LPBNPs and MTX-LLPBNPs was assessed using EDX and is displayed in **Fig. 4.3C-D**, respectively. The EDX spectra of MTX-LPBNPs showed the presence of carbon (46.0; wt.%), oxygen (18.68; wt.%), silicon (31.20; wt.%), phosphorous (1.27; wt.%), zinc (2.85; wt.%). While in the case of MTX-LLPBNPs, the spectra keep intact the characteristics peaks due to the above elements with different intensities as follows: carbon (51.0; wt.%), oxygen (26.36; wt.%), silicon (17.5; wt.%), phosphorous (0.96; wt.%), zinc (3.25; wt.%). Interestingly, nitrogen (0.93%) also appeared while analyzing MTX-LLPBNPs, which was merely due to the conjugation of protein, i.e., lactoferrin with MTX-LPBNPs. Further, analytical methods were also adopted to verify the SEM results.

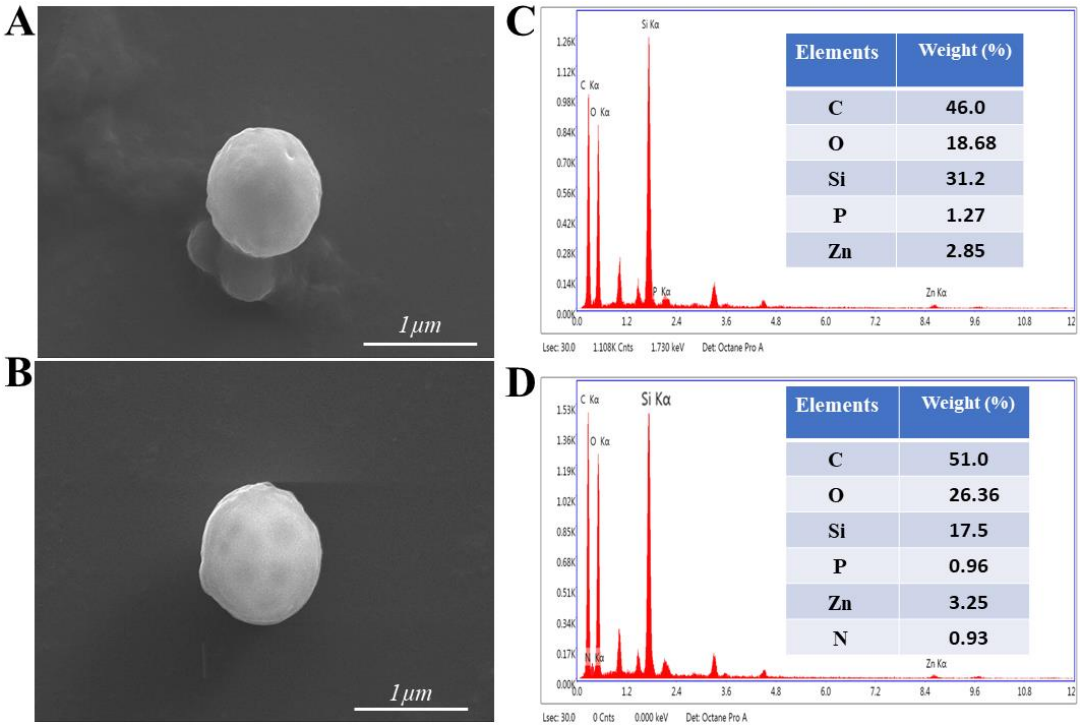

Figure 4.3. Scanning electron microscopy (SEM) photograph (A-B), and EDX images of the hybrid NPs (C-D). (A) SEM showing the MTX-LPBNPs (B) SEM showing the MTX-LLPBNPs. (C) EDX chemical mapping (inlet) and elemental composition for elements presence in MTX-LPBNPs (D) EDX chemical mapping (inlet) and elemental composition for elements presence in MTX-LLPBNPs.

3.3. Powder X-ray characterization of hybrid-nano-bioconjugate

To further characterize the NPs differentially, Powder X-ray diffraction studies were conducted for LPBNPs and MTX-LLPBNPs systems in separate experiments. The X-ray scanning was made over 2θ extending from 10° to 80°. The diffractogram showed a characteristic peak at 2θ = 27.62° for LPBNPs (**Fig. 4.4A**). The characteristics peak observed for nano-hybrid formulation is due to PCL monomer which forms a compact structure inside the system. However, broader or no characteristics peaks were observed for bare lipid NPs in comparison to N-acetyl D-glucosamine decorated nano lipid-based NPs as shown in our previous work **[32]**. Further, the polymer network facilitates the NPs system into a crystalline structure **[30]**. Interestingly, the sharp diffraction peaks were observed at 2θ = 12.50°,15.76°, 24.32°, and 27.06° for the MTX-LLPBNPs system (**Fig. 4.4B**). The diffractogram of the conjugated NPs indicates that the drugs and lactoferrin molecules show greater crystallinity. The aforementioned characterization suggests the successful conjugation of lactoferrin and MTX entrapment to the LPBNPs.

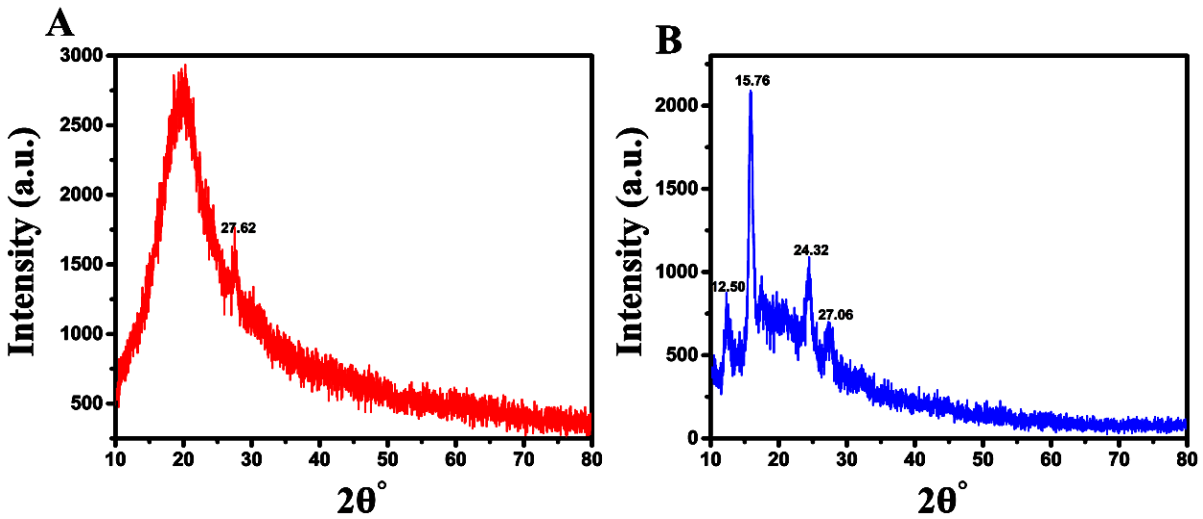

Figure 4.4. X-ray diffractograms of the hybrid system, scanning over 2θ = 10° to 2θ = 80° at a scanning speed of 0.03°/second using Cu Ka radiation (λ=1.54Å) (A) LPBNPs and (B) MTX-LLPBNPs.

3.4. Infrared spectroscopy analysis of hybrid-nano-bioconjugate

Infrared spectroscopy analysis was conducted to examine various functional groups and their interactions in the MTX-LPBNPs (Red curve) and MTX-LLPBNPs (Blue curve) system (**Fig. 4.5)**. In the red curve**,** numerous peaks were observed at 3377 cm^{-1}, 2911 cm^{-1}, 1734 cm^{-1},1436 cm^{-1}, 1371 cm^{-1},1217 cm^{-1} and 1057 cm^{-1}, which attributes to OH, CH_2 (asymmetric stretch), C=O (acid stretch), -O-C-O-, C-O (Stretching), C-O-C (ether) and PO_4^{3-}, respectively. These peaks obtained around the signature regions were due to the intrinsic functionalities of lipid, PCL, and MTX in the tested system **[33,34]**. Further, in the blue curve, the spectra keep intact the characteristic peaks due to OH, CH_2 (asymmetric stretch), C=O (acid stretch), -O-C-O-, C-O (Stretching), C-O-C (ether), and PO_4^{3-}, while the transmittance of peaks got reduced with the shifted band. Moreover, new peaks were observed in the spectrum of the fingerprint region between 1600 cm^{-1} - 1700 $cm^{-1,}$ *i.e.*, amide I (1635 cm^{-1}) and Amide II (1616 cm^{-1}). More precisely, peaks in this region were generated due to the successful conjugation of lactoferrin onto the surface of LPBNPs. The absence of C=O (acid stretch) at the wavenumber around 1734 cm^{-1} further confirms that it may involve making a bond with the amino group of the lactoferrin. The above interactions between functionalities suggest the successful formulation of MTX-LLPBNPs.

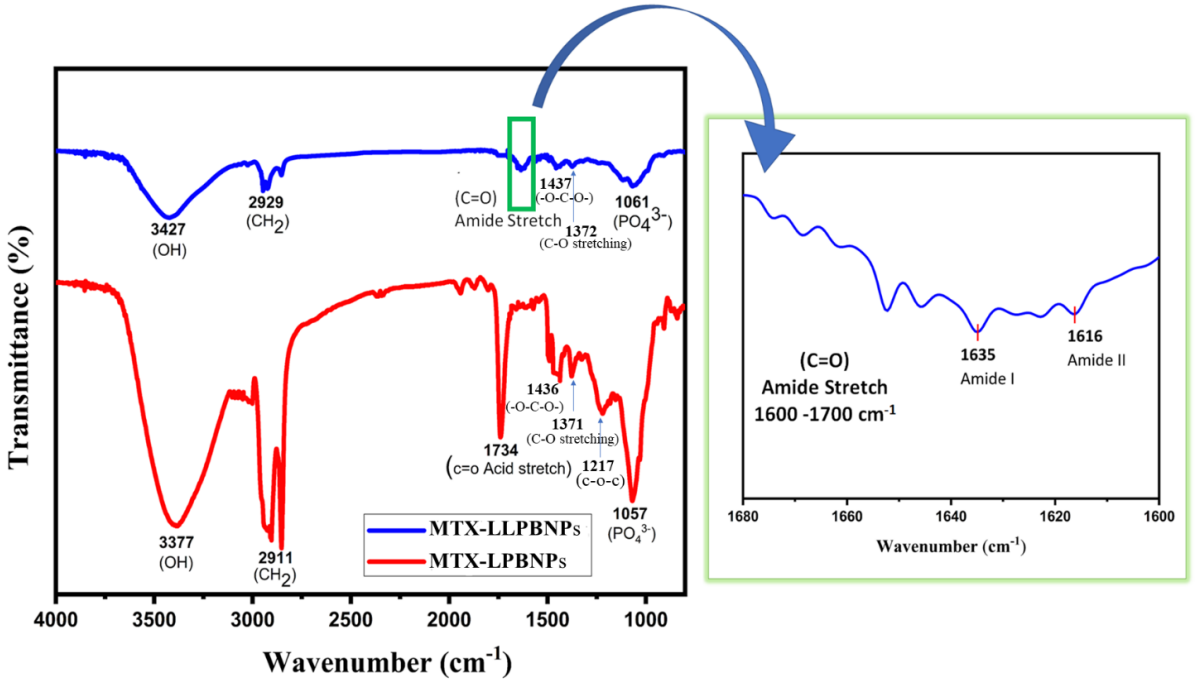

Figure 4.5. The infrared spectrum of MTX-LPBNPs (Red curve) and MTX-LLPBNPs (Blue curve); was scanned on a scale of 4000 cm^{-1} to 800 cm^{-1} with a resolution of 4 cm^{-1}.

3.5. *In vitro* drug dissociation kinetics

After characterizing the fabricated nano bioconjugate, we further investigated the drug dissociation in PBS **(Fig. 4.6)**. Zero and first-order kinetic models were applied to describe the nature of drugs dissociation from fabricated nano bioconjugate. Zero and first-order curves were obtained using equation 3 and equation 4, respectively:

$$X_t = X_0 - k_0 t \ldots\ldots\ldots\ldots\ldots Eq.\ 3$$

where, X_t, X_0, and K_0 denote cumulative % of drugs dissociation at particular time t (hour), cumulative % of drugs dissociation at time zero (hour), and kinetic constants, respectively.

$$Log\ X_t = LogX_0 - \frac{Kt}{2.303} \ldots\ldots\ldots Eq.\ 4$$

where Log X_t, Log X_0, and K denote log remaining % of drugs released at a particular time(hour), and log remaining % of drug dissociation at time zero (hour), and kinetic constants, respectively.

The dissociation curve reveals that the cumulative percent of drug release reached 28.0 ± 1.6% in the early 20.0 h. The relatively faster drugs dissociation from nano bioconjugate may be due to a certain amount of drugs adsorbed through a weak bond on the surface of the lipid **[32]**. The cancer cell can be suppressed in a very short time through an early burst of the system. Further, the cumulative percent of drug release reached only 72.0 ± 3.2% in the following 140.0 h. The release kinetic graph shows that more than 200 h is required for 100% drug release, proving its efficacy of better sustain release. On the other hand, 100 % of drugs released within 200.0 h or drug release rate hampered in other nanohybrid formulations at neutral pH **[6,35,36]**. In other words, it is also possible to discuss that this kind of release pattern is merely due to polymer at the core of the shell and lipid layer made up of lecithin and stearic acid surrounding the polymeric core. This system acts as a rate-limiting membrane that facilitates the controlled and sustained release of the drug in the *in vitro* model **[37]**. Also, the polymer network may facilitate the slow rate of drugs diffusion to the lipid layer as a result of the dissociation rate being hampered. The relatively slow rate of drug release accompanying the constructed nano-formulation is stable over time **[38]**. Such a sustained drug delivery system may offer an effective therapeutic module for cancer cells due to a prolonged drug release profile. The linear regression analysis was applied to compare the constructive drugs release pattern between the two models. Based on effective drugs dissociation from the nano-bio-conjugates, the regression equation for the zero-order curve is expressed as effective cumulative % of drug release (Dre) = 5.00 (± 2.120) + 0.326 (± 0.017) Time], with a coefficient of determinants (R^2) of 0.921. Whereas, regression equation for the first order curve is expressed as: effective Log remaining % of drug release (LDre) = 1.962 (± 0.027) + - 0.395 (± 0.0002) [Time] with a coefficient of determinants (R^2) of 0.960. The relatively higher R^2 value signifies that the model is best fitted for the first-order kinetic model, which means drug dissociation is a concentration-dependent phenomenon. The aforementioned drug delivery system facilitates drug dissociations in

sustained and controlled manner. Such a system may overcome multiple drug resistance in the diverse biological field.

Table 4.2. Storage stability performance of optimized MTX-LLPBNPs

	Storage conditions	**% Encapsulation efficiency**	**Particle size (nm)**	**PDI ± SD**	**Zeta potential (mV) ± SD**
Initial 1 month	4°C	84.0 ± 3.2%	650.7 ± 4.9	0.163 ± 0.03	-20.72 ± 1.23
	25°C/60%RH	83.6 ± 2.8%	652.7 ± 3.3	0.166 ± 0.08	-19.89 ± 0.98
		82.5 ± 3.6%	654 ± 4.8	0.194 ± 0.08	-17.10 ± 1.02
After 3 months	4°C	82.5 ± 2.3%	653.6 ± 2.8	0.168 ± 0.10	-19.09 ± 1.03
	25°C/60%RH	79.0 ± 2.60%	659.7 ± 3.1	0.201 ± 0.19	-16.09 ± 1.82

3.6. Storage stability performance

Physical and chemical stability is one of the essential parameters in the storage of the final hybrid-nano-biconjugate. Physical factors such as humidity, temperature, etc.; affect the system's stability and cause leaching of the drugs from the polymer and lipid layer. The formulated MTX-LLPBNPs were tested during 1- and 3-month periods at different storage conditions of 4 °C and 25 °C/60 %.RH. The storage stability performance of the system was determined in terms of % encapsulation efficiency, particle size, PDI, and zeta potential. The details of the detected value of stability parameters for the triplicate analysis for final formulation have been represented in **Table 4.2**. The obtained data revealed that the formulation keep maintain its physical stability at 4 °C, and no significant difference is observed during the mentioned storage period. On the other hand, MTX-LLPBNPs deteriorate their physical stability, and the value for stability parameters is significantly changed at 25 °C/60 % RH after 3 months of storage. It is interpreted from the aforementioned results that the stability of the formulations is the function of the temperature and humidity of the storage conditions **[29]**.

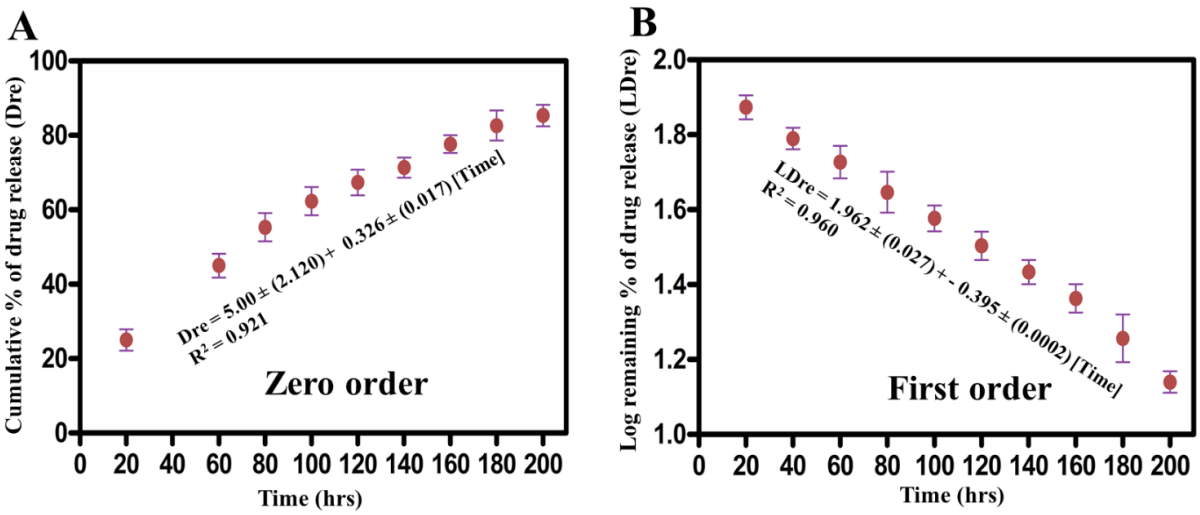

Figure 4.6. The MTX release profile of constructed hybrid nano-bioconjugate (LLPBNPs) was performed for 200 h. Dialysis was performed against phosphate buffer saline (pH 7.4) at room temperature using a dialysis bag. UV spectrophotometer was used to quantify the amounts of MTX concentration. Data are reported as (mean ± standard error) and significance level as ($p \leq 0.05*$) (**A**) zero-order kinetics and (**B**) first-order kinetics.

3.7. Study of cell toxicity

Cell toxicity induced by LPBNPs, MTX, MTX-LPBNPs, and MTX-LLPBNPs was conducted using the MTT test considering shorter incubation (**Fig. 4.7**) for 24.0 h and longer incubation (**Fig. 4.8**) for 48.0 h. Briefly, MCF-7 cells were treated with five groups of inducers (LPBNPs, free MTX, MTX-LPBNPs, and MTX-LLPBNPs) and the first to the fifth group; the MTX concentration was 2.0, 4.0, 6.0, 8.0, and 10.0 µg/mL. While in the formulation of the MTX-LPBNPs and MTX-LLPBNPs, the MTX concentration was similar to that was taken in the free form of MTX for shorter and longer incubation. LPBNPs without drug loading were taken as the negative control in the experiment, showing the maximum percent of cell viability in shorter and longer incubation. Further, cells induced with free MTX at similar concentrations, where the percentage of viable cells were observed to be 81.67 ± 1.90%, 74.07 ± 2.94%, 69.33 ± 3.10%, 66.33 ± 2.51%, and 56.03 ± 4.08%, respectively after shorter incubation. Interestingly, the viability of the cells was observed to be 70.67 ± 2.13%, 63.67 ± 1.04%, 57.33 ± 0.97%,

50.67 ± 1.90%, and 40.31 ± 2.11% at similar concentrations of free MTX after long incubation as shown in **Fig. 4.8**. For the cytotoxicity of MTX-LPBNPs formulation, similar concentrations of MTX were applied and examined for both short and long incubation times. Subsequently, cells induced with MTX-LPBNPs, the percentage of viability was found to be 90.19 ± 5.20%, 85.34 ± 2.80%, 82.67 ± 6.80%, 80.09 ± 1.70%, and 77.09 ± 5.70% after shorter incubation. However, the percentage of viability was reduced to 85.13±3.10%, 83.09 ± 5.80%, 80.14 ± 3.50%, 75.17 ± 4.50%, and 67.05 ± 1.90% after a longer incubation. In the MTX-LLPBNPs formulation, similar concentrations of MTX encapsulated, and cell cytotoxicity was examined. After, 24.0 h of incubation, the percentage of viable cells were found to be 84.77 ± 0.69%, 79.33 ± 2.09%, 74.67 ± 2.01%,71.33 ± 1.98%, and 66.0 ± 3.12%, respectively. Remarkably, after 48.0 h of incubation, the viability of the cells was reduced to 76.04 ± 2.18%, 74.02 ± 1.51%, 70.01 ± 1.11%, 63.33 ± 2.22%, and 54.03 ± 0.34% at similar concentrations of MTX. Further, we also evaluated the effect of inducers (LPBNPs, MTX, MTX-LPBNPs, and MTX-LLPBNPs) on the non-cancerous cells in the group at similar concentrations to assess their cell toxicity. Results suggest that the percent of cell viability was significantly higher for the nano-formulations than MTX (figure not shown). Furthermore, MTX-LLPBNPs formulation in comparison with free MTX reduces cell toxicity, however, the value of significance is higher at higher concentrations of drugs for both shorter and longer incubation periods. From the above investigation, it can be concluded that free MTX was more lethal to MCF-cells than formulated NPs *in vitro* conditions because small molecules can be easily traveled across the plasma membrane via passive diffusion **[39]**. It is also observed that MTX-LLPBNPs induce more cytotoxicity than MTX-LPBNPs at all the concentrations and incubations. The enhanced efficacy mechanism of cell toxicity of MX-LLPBNPs results from ligand lactoferrin binds to the specific receptor expressed on the cell surface of the MCF-7 **[14]**. Obtained results are consistent compared to the previous studies considering other drug delivery systems **[40]**.

Furthermore, It can be concluded that LLPBNPs formulation favors the control and constant rate of drug release over a long period. Through such hybrid-nano-bioconjugate, the maximum tolerated dose of drugs can be increased for the effective therapy of cancer. Since higher concentrations of drugs, when exposed in the free form, may be toxic to normal cells in the blood circulation **[41]**. However, cell toxicity was found maximum for free MTX to formulations, which means achieving a better therapeutic effect and maximum tolerated dose; the drugs should be formulated in the LLPBNPs system. Further, a quantitative evaluation of the therapeutic potential of the dosages, the parameter IC50, is required. The following linear equation was used to calculate IC50:

$$\mathrm{IC50} = (0.5 - b)/a \qquad \ldots\ldots\ldots\ldots\ldots\ldots \textit{Eq. 5}$$

Where a and b denote slope and intercept, respectively.

The IC50 value was found to be 17.4 ± 1.10 µg/mL, and 13.4 ± 1.14 µg/mL for MTX-LLPBNPs after 24.0 h and 48.0 h of incubation, respectively.

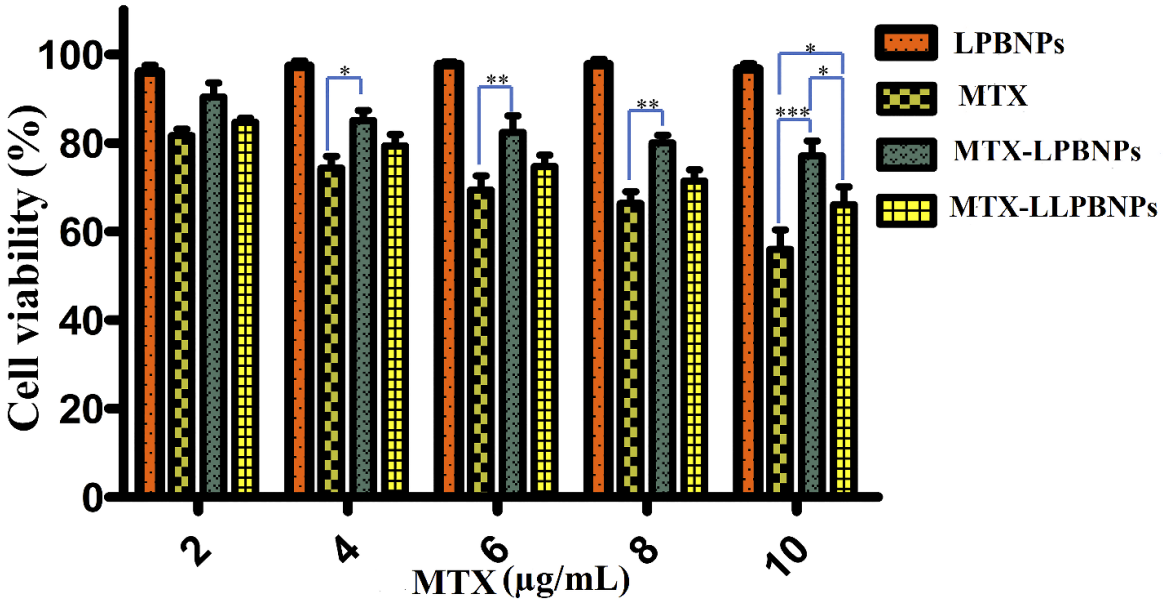

Figure 4.7. Cell toxicity studies of LPBNPs, MTX, MTX-LPBNPs, and MTX-LLPBNPs on MCF-7 for 24.0 h of incubation. Treatment was studied in the five groups. In the first, second, third, fourth, and fifth groups, the MTX concentration was taken 2.0, 4.0, 6.0, 8.0, and 10.0 µg/mL, respectively. In the MTX-LPBNPs and MTX-LLPBNPs formulation, a similar concentration of MTX was taken in each group. However, the LPBNPs were taken as a control in the groups. Values are reported as (mean ± standard error) and significance level as ($^{***}p< 0.001$, $^{**}p<0.01$ and $^{*}p<0.05$).

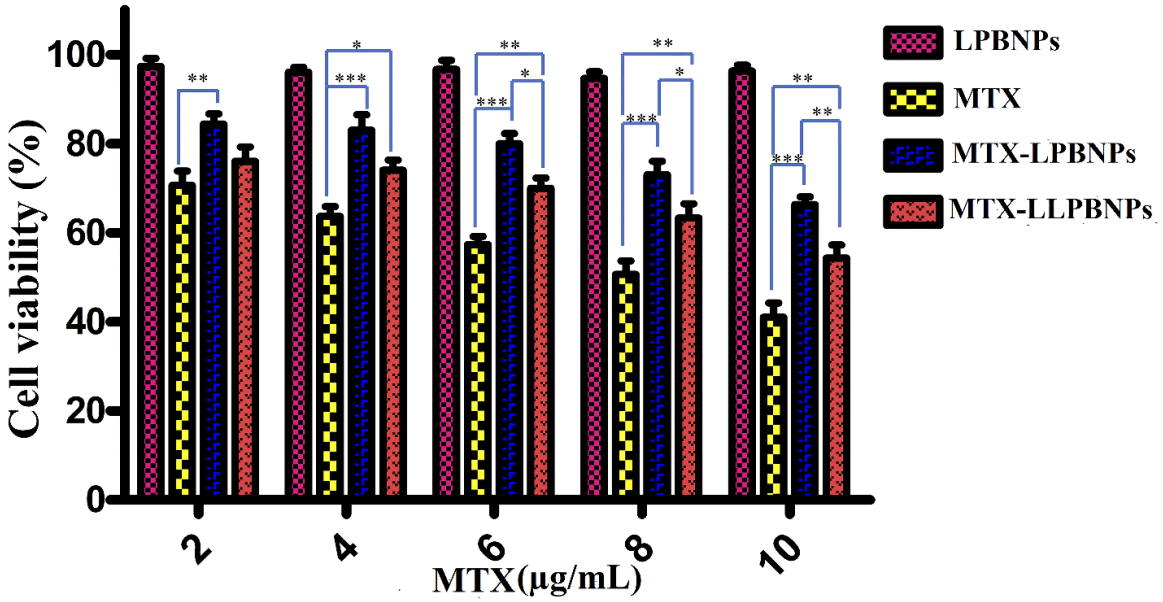

Figure 4.8. Cell toxicity studies of LPBNPs, MTX, MTX-LPBNPs, and MTX-LLPBNPs on MCF-7 for 48.0 h of incubation. Treatment was studied in the five groups. In the first, second, third, fourth, and fifth groups, the MTX concentration was taken 2.0, 4.0, 6.0, 8.0, and 10.0 µg/mL, respectively. In the MTX-LPBNPs and MTX-LLPBNPs formulation, a similar concentration of MTX was taken in each group. However, the LPBNPs were taken as a control in the groups. Values are reported as (mean ± standard error) and significance level as ($^{***}p< 0.001$, $^{**}p<0.01$ and $^{*}p<0.05$).

3.8. Morphological analysis of MCF-7 cells induced with LPBNPs / MTX-LPBNPs / MTX-LLPBNPs

The bioimaging of the cells was conducted to validate the morphological changes induced with LPBNPs, and the LLPBNPs system and comparisons are drawn between them. The morphological changes of the formulations were studied using fluorescence microscopy after a shorter (24.0 h) and longer (48.0 h) incubation period. The fluorescence signals from the cells are illustrated in **Fig. 4.9-4.10**. The images obtained from DAPI staining display the blue fluorescence signals from the nucleus of the cells **(Fig. 4.9-A** and **Fig. 4.10-A)**. However, the red fluorescence signals from rhodamine-conjugated phalloidin staining show the cytoskeleton of the cells **(Fig. 4.9-B** and **Fig. 4.10-B)**. Moreover, fluorescence signals from images (**Fig.**

4.9-C) and (**Fig. 4.10-C**) are a consequence of merge channels of DAPI and rhodamine-conjugated phalloidin. LLPBNPs induced time-dependent fluorescence intensity in the nucleus and cytoskeleton of the cells, indicating more accumulation of the drugs. Similar results have been reported for other drug delivery systems, proving the formulated system's efficacy [24]. Furthermore, cells treated with LPBNPs (Row 1) stabilized a large and clear nucleus after a shorter and longer incubation. The above findings suggest that the LPBNPs are biocompatible and suitable for biological applications. Further, compared to MTX- LPBNPs (Row 2), MTX-LLPBNPs (Row 3) induce more cell shrinkage with nuclear fragmentation after a shorter and longer incubation. Moreover, nuclei of the cells got smaller and elongated with an un-organized cytoskeleton comparatively after a shorter and longer treatment period. However, when comparing our results with previously reported results, the developed LLPBNPs formulation induces significant morphological changes at even lower concentrations of drugs **[21,40]**. The cellular basis of internalization of LPBNPs is presumed to be cell fusion followed by carrier-mediated endocytosis **[41]**. The phospholipids (e.g., phosphatidylserine and phosphatidylcholine) are an integral part of the cell membrane. They organize differently and surround the cytoplasm and nucleus to facilitate selective interactions with the cellular environment **[42]**. In the formulation of LPBNPs, phospholipids may facilitate the intake of the drugs through interactions between carriers and the cell membrane. However, LLPBNPs facilitate changing cellular morphology comparatively more than can be assumed as nano formulations support receptor-mediated drug delivery **[43]**. Henceforth it can be concluded LLPBNP is an excellent drug delivery vehicle in MCF-7 cells that enhances cellular toxicity of the drug as compared to LPBNPs.

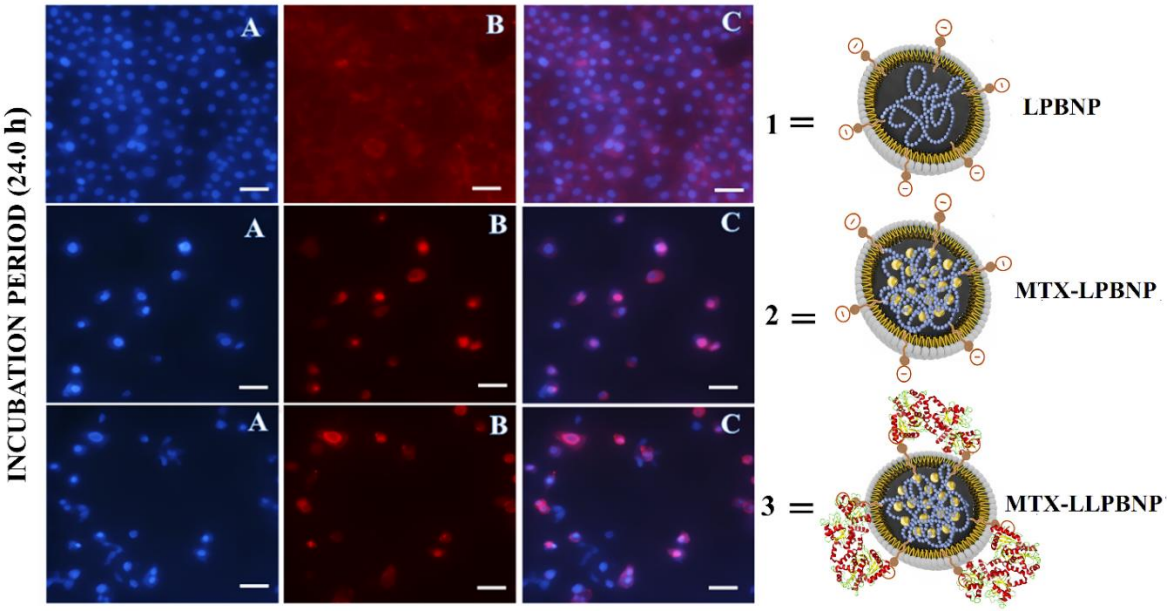

Figure 4.9. Fluorescence microscopy photographs of the MCF-7 after 24.0 h of treatment with LPBNPs, MTX-LPBNPs, and MTX-LLPBNPs at equivalent MTX, 10.0 (µg/mL). The fluorescence signals from the cells were illustrated in **Row 1-3** after 24.0 h of incubation. (**Row1-A**) DAPI staining, blue signals show the nucleus induced with LPBNPs. (**Row 1-B**) rhodamine-conjugated phalloidin staining, red signals show the cytoskeleton induced with LPBNPs. (**Row 1-C**) merged distribution of DAPI & rhodamine-conjugated phalloidin. (**Row 2-A**) DAPI staining, blue signals show the nucleus induced with MTX-LPBNPs. (**Row 2-B**) rhodamine-conjugated phalloidin staining, red signals show the cytoskeleton induced with MTX-LPBNPs. (**Row 2-C**) merged distribution of DAPI & rhodamine-conjugated phalloidin. (**Row 3-A**) DAPI staining, blue signals show the nucleus induced with LLPBNPs. (**Row 3-B**) rhodamine-conjugated phalloidin staining, red signals show cytoskeleton induced with MTX-LLPBNPs. (**Row 3-C**) merged distribution of DAPI & rhodamine-conjugated phalloidin. The scale bar is 50 µm for fluorescence images

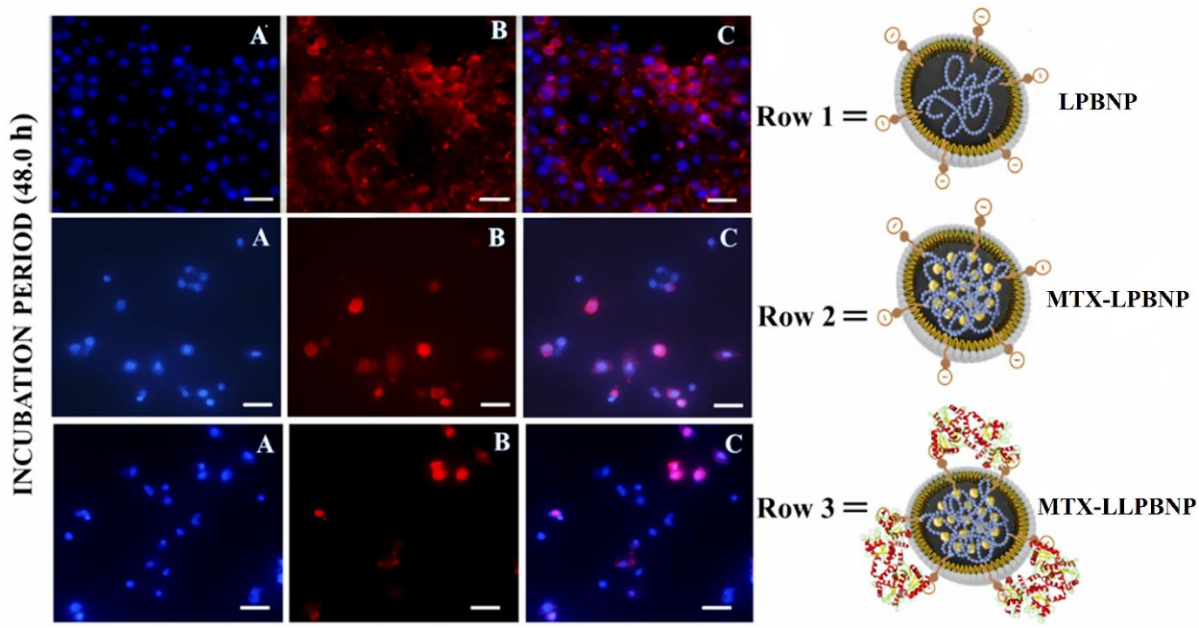

Figure 4.10. Fluorescence microscopy photographs of the MCF-7 after 48.0 h of treatment with LPBNPs, MTX-LPBNPs, and MTX-LLPBNPs at equivalent MTX, 10.0 (µg/mL). The fluorescence signals from the cells were illustrated in **Row 1-3** after 48.0 h of incubation. (**Row1-A**) DAPI staining, blue signals show the nucleus induced with LPBNPs. (**Row 1-B**) rhodamine-conjugated phalloidin staining, red signals show the cytoskeleton induced with LPBNPs. (**Row 1-C**) merged distribution of DAPI & rhodamine-conjugated phalloidin. (**Row 2-A**) DAPI staining, blue signals show the nucleus induced with MTX-LPBNPs. (**Row 2-B**) rhodamine-conjugated phalloidin staining, red signals show the cytoskeleton induced with MTX-LPBNPs. (**Row 2-C**) merged distribution of DAPI & rhodamine-conjugated phalloidin. (**Row 3-A**) DAPI staining, blue signals show the nucleus induced with LLPBNPs. (**Row 3-B**) rhodamine-conjugated phalloidin staining, red signals show cytoskeleton induced with MTX-LLPBNPs. (**Row 3-C**) merged distribution of DAPI & rhodamine-conjugated phalloidin. The scale bar is 50 µm for fluorescence images.

4. Conclusion

In the present investigation, a lactoferrin-conjugated NP of a composite of lipid armor and polymer interior was effectively constructed via a one-step nanoprecipitation technique. In the design, the lipid monomer that surrounds the polymer network facilitates the NPs with similar characteristics as intact in the plasma membrane of the cells. Further, the formulated construct containing stearic acid provides the moieties for ligand conjugation and stabilizes hybrid NPs. Such a hybrid formulation may protect the drugs from being degraded while circulation in the reticuloendothelial system with sustained, controlled, and targeted delivery of MTX in lactoferrin overexpressed cancer cells. In addition, a network of polymer imparts the nano-carriers with stability, crystallinity, improving encapsulation efficiency, and controlling drug delivery. Data obtained from the above experiment may pave the way towards overcoming the multiple drugs resistance that requires prolonged treatment modules using the constructed hybrid-nano-bioconjugate. Hence, it is a concept-based investigation of composite material of the lipid-polymer structural component. Further, *in vivo* studies to be undertaken of constructed hybrid-nano-bioconjugate to collect sufficient information and results for pre-clinical trials.

5. References

[1] K. Cho, X. Wang, S. Nie, Z. (Georgia) Chen, D.M. Shin, Therapeutic Nanoparticles for Drug Delivery in Cancer, Clin Cancer Res. 14 (2008) 1310–1316. https://doi.org/10.1158/1078-0432.CCR-07-1441.

[2] C. Clawson, L. Ton, S. Aryal, V. Fu, S. Esener, L. Zhang, Synthesis and Characterization of Lipid–Polymer Hybrid Nanoparticles with pH-Triggered Poly(ethylene glycol) Shedding, Langmuir. 27 (2011) 10556–10561. https://doi.org/10.1021/la202123e.

[3] Sophie Bou,1, Xinyue Wang,2, Nicolas Anton,2, Redouane Bouchaala,1, Andrey S. Klymchenko,1, Mayeul, Collot1*, Lipid-Core/Polymer-Shell Hybrid Nanoparticles: Synthesis and Characterization by Fluorescence Labeling and Electrophoresis, (2020) 1–9. https://doi.org/10.1039/D0SM00077A.

[4] W. Ge, Gao, Li, Yang, Fang, Han, Wang, Nanomaterials in the application of tumor vaccines: advantages and disadvantages, OTT. (2013) 629. https://doi.org/10.2147/OTT.S41902.

[5] R. Singh, H.S. Nalwa, Medical Applications of Nanoparticles in Biological Imaging, Cell Labeling, Antimicrobial Agents, and Anticancer Nanodrugs, J Biomed Nanotechnol. 7 (2011) 489–503. https://doi.org/10.1166/jbn.2011.1324.

[6] J.M. Chan, L. Zhang, K.P. Yuet, G. Liao, J.-W. Rhee, R. Langer, O.C. Farokhzad, PLGA–lecithin–PEG core–shell nanoparticles for controlled drug delivery, Biomaterials. 30 (2009) 1627–1634. https://doi.org/10.1016/j.biomaterials.2008.12.013.

[7] K.S. Soppimath, D.C.-W. Tan, Y.-Y. Yang, pH-Triggered Thermally Responsive Polymer Core-Shell Nanoparticles for Drug Delivery, Adv. Mater. 17 (2005) 318–323. https://doi.org/10.1002/adma.200401057.

[8] V.P. Torchilin, Recent advances with liposomes as pharmaceutical carriers, Nat Rev Drug Discov. 4 (2005) 145–160. https://doi.org/10.1038/nrd1632.

[9] S. Vyas, S. Rai, R. Paliwal, P. Gupta, K. Khatri, A. Goyal, B. Vaidya, Solid Lipid Nanoparticles (SLNs) as a Rising Tool in Drug Delivery Science: One Step Up in Nanotechnology, CNANO. 4 (2008) 30–44. https://doi.org/10.2174/157341308783591816.

[10] R. Tong, J. Cheng, Anticancer Polymeric Nanomedicines, Polymer Revs. 47 (2007) 345–381. https://doi.org/10.1080/15583720701455079.

[11] K. Baumgarten, B.P. Tighe, Viscous forces and bulk viscoelasticity near jamming, Soft Matter. 13 (2017) 8368–8378. https://doi.org/10.1039/C7SM01619K.

[12] H.L. Wong, R. Bendayan, A.M. Rauth, H.Y. Xue, K. Babakhanian, X.Y. Wu, A Mechanistic Study of Enhanced Doxorubicin Uptake and Retention in Multidrug Resistant Breast Cancer Cells Using a Polymer-Lipid Hybrid Nanoparticle System, J Pharmacol Exp Ther. 317 (2006) 1372–1381. https://doi.org/10.1124/jpet.106.101154.

[13] H.L. Wong, R. Bendayan, A.M. Rauth, X.Y. Wu, Simultaneous delivery of doxorubicin and GG918 (Elacridar) by new Polymer-Lipid Hybrid Nanoparticles (PLN) for enhanced treatment of multidrug-resistant breast cancer, Journal of Controlled Release. 116 (2006) 275–284. https://doi.org/10.1016/j.jconrel.2006.09.007.

[14] N.N. Palei, B.C. Mohanta, M.L. Sabapathi, M.K. Das, Lipid-based nanoparticles for cancer diagnosis and therapy, in: Organic Materials as Smart Nanocarriers for Drug Delivery, Elsevier, 2018: pp. 415–470. https://doi.org/10.1016/B978-0-12-813663-8.00010-5.

[15] E.S. Lee, K. Na, Y.H. Bae, Polymeric micelle for tumor pH and folate-mediated targeting, Journal of Controlled Release. (2003) 11.

[16] H. Nosrati, A. Mojtahedi, H. Danafar, H. Kheiri Manjili, Enzymatic stimuli-responsive methotrexate-conjugated magnetic nanoparticles for target delivery to breast cancer cells and release study in lysosomal condition: ENZYMATIC STIMULI-RESPONSIVE MTX, J. Biomed. Mater. Res. 106 (2018) 1646–1654. https://doi.org/10.1002/jbm.a.36364.
[17] M. Choudhary, P. Yadav, A. Singh, S. Kaur, J. Ramirez-Vick, P. Chandra, K. Arora, S.P. Singh, CD 59 Targeted Ultrasensitive Electrochemical Immunosensor for Fast and Noninvasive Diagnosis of Oral Cancer, Electroanalysis. 28 (2016) 2565–2574. https://doi.org/10.1002/elan.201600238.
[18] M.H. Akhtar, K.K. Hussain, N.G. Gurudatt, P. Chandra, Y.-B. Shim, Ultrasensitive dual probe immunosensor for the monitoring of nicotine induced-brain derived neurotrophic factor released from cancer cells, Biosensors and Bioelectronics. 116 (2018) 108–115. https://doi.org/10.1016/j.bios.2018.05.049.
[19] P. Chandra, W.C.A. Koh, H.-B. Noh, Y.-B. Shim, In vitro monitoring of i-NOS concentrations with an immunosensor: The inhibitory effect of endocrine disruptors on i-NOS release, Biosensors and Bioelectronics. 32 (2012) 278–282. https://doi.org/10.1016/j.bios.2011.11.027.
[20] K. Mahato, B. Purohit, A. Kumar, P. Chandra, Clinically comparable impedimetric immunosensor for serum alkaline phosphatase detection based on electrochemically engineered Au-nano-Dendroids and graphene oxide nanocomposite, Biosensors and Bioelectronics. 148 (2020) 111815. https://doi.org/10.1016/j.bios.2019.111815.
[21] B. Wu, P. Yu, C. Cui, M. Wu, Y. Zhang, L. Liu, C.-X. Wang, R.-X. Zhuo, S.-W. Huang, Folate-containing reduction-sensitive lipid–polymer hybrid nanoparticles for targeted delivery of doxorubicin, Biomater. Sci. 3 (2015) 655–664. https://doi.org/10.1039/C4BM00462K.
[22] C.-E. Kim, S.-K. Lim, J.-S. Kim, In vivo antitumor effect of cromolyn in PEGylated liposomes for pancreatic cancer, Journal of Controlled Release. 157 (2012) 190–195. https://doi.org/10.1016/j.jconrel.2011.09.066.
[23] N.K. Garg, B. Singh, A. Jain, P. Nirbhavane, R. Sharma, R.K. Tyagi, V. Kushwah, S. Jain, O.P. Katare, Fucose decorated solid-lipid nanocarriers mediate efficient delivery of methotrexate in breast cancer therapeutics, Colloids and Surfaces B: Biointerfaces. 146 (2016) 114–126. https://doi.org/10.1016/j.colsurfb.2016.05.051.
[24] M. Hamdi, H.M. Abdel-Bar, E. Elmowafy, K.T. Al-Jamal, G.A.S. Awad, An integrated vitamin E-coated polymer hybrid nanoplatform: A lucrative option for an enhanced in vitro macrophage retention for an anti-hepatitis B therapeutic prospect, PLoS ONE. 15 (2020) e0227231. https://doi.org/10.1371/journal.pone.0227231.
[25] H. Hu, D. Liu, X. Zhao, M. Qiao, D. Chen, Preparation, characterization, cellular uptake and evaluation *in vivo* of solid lipid nanoparticles loaded with cucurbitacin B, Drug Development and Industrial Pharmacy. 39 (2013) 770–779. https://doi.org/10.3109/03639045.2012.702348.
[26] C.T. Sengel-Turk, C. Hascicek, F. Bakar, E. Simsek, Comparative Evaluation of Nimesulide-Loaded Nanoparticles for Anticancer Activity Against Breast Cancer Cells, AAPS PharmSciTech. 18 (2017) 393–403. https://doi.org/10.1208/s12249-016-0514-2.
[27] H. Nosrati, M. Salehiabar, S. Davaran, H. Danafar, H.K. Manjili, Methotrexate-conjugated L-lysine coated iron oxide magnetic nanoparticles for inhibition of MCF-7 breast cancer cells, Drug Development and Industrial Pharmacy. 44 (2018) 886–894. https://doi.org/10.1080/03639045.2017.1417422.
[28] S. Feng, G. Huang, Effects of emulsifiers on the controlled release of paclitaxel (Taxol®) from nanospheres of biodegradable polymers, Journal of Controlled Release. (2001) 17.

[29] C.T. Sengel-Turk, N. Ozmen, F. Bakar-Ates, Design, characterization and evaluation of cucurbitacin B-loaded core–shell-type hybrid nano-sized particles using DoE approach, Polym. Bull. 78 (2021) 3327–3351. https://doi.org/10.1007/s00289-020-03256-7.
[30] A.L. Sisson, D. Ekinci, A. Lendlein, The contemporary role of ε-caprolactone chemistry to create advanced polymer architectures, Polymer. 54 (2013) 4333–4350. https://doi.org/10.1016/j.polymer.2013.04.045.
[31] Y. Sheng, L. Chang, T. Kuang, J. Hu, PEG/heparin-decorated lipid–polymer hybrid nanoparticles for long-circulating drug delivery, RSC Adv. 6 (2016) 23279–23287. https://doi.org/10.1039/C5RA26215A.
[32] R. Kumar, Divya, S. Mahapatra, V.K. Dubey, P. Chandra, N-acetyl-d-glucosamine decorated nano-lipid-based carriers as theranostics module for targeted anti-cancer drug delivery, Materials Chemistry and Physics. 282 (2022) 125956. https://doi.org/10.1016/j.matchemphys.2022.125956.
[33] R. Kumar, D.K. Choudhary, M. Debnath, Development of BSA conjugated on modified surface of quercetin- loaded lipid nanocarriers for breast cancer treatment, Mater. Res. Express. 7 (2020) 015411. https://doi.org/10.1088/2053-1591/ab6774.
[34] K. Rostamizadeh, M. Manafi, H. Nosrati, H. Kheiri Manjili, H. Danafar, Methotrexate-conjugated mPEG–PCL copolymers: a novel approach for dual triggered drug delivery, New J. Chem. 42 (2018) 5937–5945. https://doi.org/10.1039/C7NJ04864E.
[35] L. Zhang, J.M. Chan, F.X. Gu, J.-W. Rhee, A.Z. Wang, A.F. Radovic-Moreno, F. Alexis, R. Langer, O.C. Farokhzad, Self-Assembled Lipid−Polymer Hybrid Nanoparticles: A Robust Drug Delivery Platform, ACS Nano. 2 (2008) 1696–1702. https://doi.org/10.1021/nn800275r.
[36] F. Bakar-Ates, E. Ozkan, C.T. Sengel-Turk, Encapsulation of cucurbitacin B into lipid polymer hybrid nanocarriers induced apoptosis of MDAMB231 cells through PARP cleavage, International Journal of Pharmaceutics. 586 (2020) 119565. https://doi.org/10.1016/j.ijpharm.2020.119565.
[37] V. Dave, R.B. Yadav, K. Kushwaha, S. Yadav, S. Sharma, U. Agrawal, Lipid-polymer hybrid nanoparticles: Development & statistical optimization of norfloxacin for topical drug delivery system, Bioactive Materials. 2 (2017) 269–280. https://doi.org/10.1016/j.bioactmat.2017.07.002.
[38] L.N.M. Ribeiro, A.C.S. Alcântara, G.H. Rodrigues da Silva, M. Franz-Montan, S.V.G. Nista, S.R. Castro, V.M. Couto, V.A. Guilherme, E. de Paula, Advances in Hybrid Polymer-Based Materials for Sustained Drug Release, International Journal of Polymer Science. 2017 (2017) 1–16. https://doi.org/10.1155/2017/1231464.
[39] D. Aouameur, H. Cheng, Y. Opoku-Damoah, B. Sun, Q. Dong, Y. Han, J. Zhou, Y. Ding, Stimuli-responsive gel-micelles with flexible modulation of drug release for maximized antitumor efficacy, Nano Res. 11 (2018) 4245–4264. https://doi.org/10.1007/s12274-018-2012-1.
[40] Y. Liu, K. Li, J. Pan, B. Liu, S.-S. Feng, Folic acid conjugated nanoparticles of mixed lipid monolayer shell and biodegradable polymer core for targeted delivery of Docetaxel, Biomaterials. 31 (2010) 330–338. https://doi.org/10.1016/j.biomaterials.2009.09.036.
[41] D. Manzanares, V. Ceña, Endocytosis: The Nanoparticle and Submicron Nanocompounds Gateway into the Cell, Pharmaceutics. 12 (2020) 371. https://doi.org/10.3390/pharmaceutics12040371.
[42] Y. Hu, R. Hoerle, M. Ehrich, C. Zhang, Engineering the lipid layer of lipid-PLGA hybrid nanoparticles for enhanced in vitro cellular uptake and improved stability, (2016) 21.

[43] P. Decuzzi, M. Ferrari, The role of specific and non-specific interactions in receptormediated endocytosis of nanoparticles, Biomaterials 18 (2007) 2915–2922, https://doi.org/10.1016/j.biomaterials.2007.02.013.2007.